AIAA JOURNAL
Vol. 47, No. 12, December 2009

Correlation-Based Transition Modeling for Unstructured Parallelized Computational Fluid Dynamics Codes

Robin B. Langtry*
The Boeing Company, Seattle, Washington 98124-2207
and
Florian R. Menter†
ANSYS Germany, 83624 Otterfing, Germany

DOI: 10.2514/1.42362

A new correlation-based transition model has been developed, which is built strictly on local variables. As a result, the transition model is compatible with modern computational fluid dynamics techniques such as unstructured grids and massively parallel execution. The model is based on two transport equations, one for intermittency and one for a transition onset criterion in terms of momentum-thickness Reynolds number. A number of validation papers have been published on the basic formulation of the model. However, until now the full model correlations have not been published. The main goal of the present paper is to publish the full model and release it to the research community so that it can continue to be further validated and possibly extended or improved. Included in this paper are a number of test cases that can be used to validate the implementation of the model in a given computational fluid dynamics code. The authors believe that the current formulation is a significant step forward in engineering transition modeling, as it allows the combination of transition correlations with general-purpose computational fluid dynamics codes. There is a strong potential that the model will allow the first-order effects of transition to be included in everyday industrial computational fluid dynamics simulations.

Nomenclature

C_f = skin friction coefficient, $\tau/(0.5\rho U_{\text{ref}}^2)$
k = turbulent kinetic energy
Re_x = Reynolds number, $\rho L U_{\text{ref}}/\mu$
Re_θ = momentum-thickness Reynolds number, $\rho\theta U_0/\mu$
$Re_{\theta t}$ = transition onset momentum-thickness Reynolds number (based on freestream conditions), $\rho\theta_t U_0/\mu$
$\tilde{Re}_{\theta t}$ = local transition onset momentum-thickness Reynolds number (obtained from a transport equation)
R_T = viscosity ratio
R_y = wall-distance-based turbulent Reynolds number
R_v = vorticity Reynolds number
S = absolute value of strain rate, $(2S_{ij}S_{ij})^{1/2}$
S_{ij} = strain-rate tensor, $0.5(\partial u_i/\partial x_j + \partial u_j/\partial x_i)$
Tu = turbulence intensity, $100(2k/3)^{1/2}/U$
U = local velocity
U_o = local freestream velocity
U_{ref} = inlet reference velocity
u' = local fluctuating streamwise velocity
x/C = axial distance over axial chord
y = distance to nearest wall
y^+ = distance in wall coordinates, $\rho y\mu_\tau/\mu$
δ = boundary-layer thickness
θ = momentum thickness
λ_θ = pressure gradient parameter, $(\rho\theta^2/\mu)(dU/ds)$
μ = molecular viscosity
μ_t = eddy viscosity
ρ = density
τ = wall shear stress
Ω = absolute value of vorticity, $(2\Omega_{ij}\Omega_{ij})^{1/2}$
Ω_{ij} = vorticity tensor, $0.5(\partial u_i/\partial x_j - \partial u_j/\partial x_i)$
ω = specific turbulence dissipation rate

Subscripts

s = streamline
t = transition onset

Received 24 November 2008; revision received 9 June 2009; accepted for publication 30 June 2009.

*Senior Engineer, Enabling Technology and Research, P.O. Box 3703, Mail Code 67-LF; robin.b.langtry@boeing.com.
†Development Manager, Fluids Business Unit, Staudenfeldweg 12; florian.menter@ansys.com.

I. Introduction

IN THE past few decades, a significant amount of progress has been made in the development of reliable turbulence models that can accurately simulate a wide range of fully turbulent engineering flows. The efforts by different groups have resulted in a spectrum of models that can be used in many different applications, while balancing the accuracy requirements and the computational resources available to a computational fluid dynamics (CFD) user. However, the important effect of laminar-turbulent transition is not included in the majority of today's engineering CFD simulations. The reason for this is that transition modeling does not offer the same wide spectrum of CFD-compatible model formulations that are currently available for turbulent flows, even though a large body of publications is available on the subject. There are several reasons for this unsatisfactory situation.

The first is that transition occurs through different mechanisms in different applications. In aerodynamic flows, transition is typically the result of a flow instability (Tollmien–Schlichting waves or, in the case of highly swept wings, crossflow instability), where the resulting exponential growth of two-dimensional waves eventually results in a nonlinear breakdown to turbulence. Transition occurring due to Tollmien–Schlichting waves is often referred to as natural transition [1]. In turbomachinery applications, the main transition mechanism is bypass transition [2] imposed on the boundary layer by high levels of turbulence in the freestream. The high freestream turbulence levels are for instance generated by upstream blade rows. Another important transition mechanism is separation-induced transition [3], where a laminar boundary layer separates under the influence of a pressure gradient and transition develops within the separated shear layer

(which may or may not reattach). As well, a turbulent boundary layer can relaminarize under the influence of a strong favorable pressure gradient [4]. Although the importance of transition phenomena for aerodynamic and heat transfer simulations is widely accepted, it is difficult to include all of these effects in a single model.

The second complication arises from the fact that conventional Reynolds-averaged Navier–Stokes (RANS) procedures do not lend themselves easily to the description of transitional flows, where both linear and nonlinear effects are relevant. RANS averaging eliminates the effects of linear disturbance growth and is therefore difficult to apply to the transition process. Although methods based on the stability equations such as the e^n method of Smith and Gamberoni [5] and van Ingen [6] avoids this limitation, they are not compatible with general-purpose CFD methods as typically applied in complex geometries. The reason is that these methods require a priori knowledge of the geometry and the grid topology. In addition, they involve numerous nonlocal operations (e.g., tracking the disturbance growth along each streamline) that are difficult to implement into today's CFD methods [7]. This is not to argue against the stability approaches, as they are an essential part of the desired "spectrum" of transition models required for the vastly different application areas and accuracy requirements. However, much like in turbulence modeling, it is important to develop engineering models that can be applied in day-to-day operations by design engineers on complicated 3-D geometries.

It should be noted that, at least for 2-D flows, the efforts of various groups have resulted in a number of engineering design tools intended to model transition for very specific applications. The most notable efforts are those of Drela and Giles [8] who developed the X-FOIL code which can be used for modeling transition on 2-D airfoils, and the MISES code of Youngren and Drela [9], which is used for modeling transition on 2-D turbomachinery blade rows. Both of these codes use a viscous–inviscid coupling approach which allows the classical boundary-layer formulation tools to be used. Transition prediction is accomplished using either an e^n method or an empirical correlation, and both of these codes are used widely in their respective design communities. A 3-D wing or blade design is performed by stacking the 2-D profiles (with the basic assumption that spanwise flow is negligible) to create the geometry at which point a 3-D CFD analysis is performed.

Closer inspection shows that hardly any of the current transition models are CFD compatible. Most formulations suffer from nonlocal operations that cannot be carried out (with reasonable effort) in general-purpose CFD codes. This is because modern CFD codes use mixed elements and massive parallel execution and do not provide the infrastructure for computing integral boundary-layer parameters or allow the integration of quantities along the direction of external streamlines. Even if structured boundary-layer grids are used (typically hexahedra), the codes are based on data structures for unstructured meshes. The information on a body-normal grid direction is therefore not easily available. In addition, most industrial CFD simulations are carried out on parallel computers using a domain decomposition methodology. This means in the most general case that boundary layers can be split and computed on different processors, prohibiting any search or integration algorithms. Consequently, the main requirements for a fully CFD-compatible transition model are as follows:

1) Allow the *calibrated* prediction of the onset and the length of transition.

2) Allow the inclusion of different transition mechanisms.

3) Be formulated locally (no search or line-integration operations).

4) Avoid multiple solutions (same solution for initially laminar or turbulent boundary layer).

5) Do not affect the underlying turbulence model in fully turbulent regimes.

6) Allow a robust integration down to the wall with similar convergence as the underlying turbulence model.

7) Be formulated independent of the coordinate system.

8) Be applicable to three-dimensional boundary layers.Considering the main classes of engineering transition models (stability analysis, correlation-based models, low-Re models), one finds that none of these methods can meet all of the aforementioned requirements.

The only transition models that have historically been compatible with modern CFD methods are the low-Re models [10,11]. However, they typically suffer from a close interaction with the transition capability and the viscous sublayer modeling, and this can prevent an independent calibration of both phenomena [12,13]. At best, the low-Re models can only be expected to simulate bypass transition which is dominated by diffusion effects from the freestream. This is because the standard low-Re models rely exclusively on the ability of the wall damping terms to capture the effects of transition. Realistically, it would be very surprising if these models that were calibrated for viscous sublayer damping could faithfully reproduce the physics of transitional flows. It should be noted that there are several low-Re models where transition prediction was considered specifically during the model calibration [14–16]. However, these model formulations still exhibit a close connection between the sublayer behavior and the transition calibration. Recalibration of one functionality also changes the performance of the other. It is therefore not possible to introduce additional experimental information without a substantial reformulation of the entire model.

The engineering alternative to low-Re transition models are empirical correlations such as those of [17–19]. They typically correlate the transition momentum-thickness Reynolds number to local freestream conditions such as the turbulence intensity and pressure gradient. These models are relatively easy to calibrate and are often sufficiently accurate to capture the major effects of transition. In addition, correlations can be developed for the different transition mechanisms, ranging from bypass to natural transition as well as crossflow instability or roughness. The main shortcoming of these models lies in their inherently nonlocal formulation. They typically require information on the integral thickness of the boundary layer and the state of the flow outside the boundary layer. Although these models have been used successfully in special-purpose turbomachinery codes, the nonlocal operations involved with evaluating the boundary-layer momentum thickness and determining the freestream conditions have precluded their implementation into general-purpose CFD codes.

Transition simulations based on linear stability analysis such as the e^n method are the lowest closure level available where the actual instability of the flow is simulated. In the simpler models previously described, the physics are introduced through the calibration of the model constants. However, even the e^n method is not free from empiricism. This is because the transition n factor is not universal and depends on the wind-tunnel freestream/acoustic environment and also the smoothness of the test model surface. The main obstacle to the use of the e^n model is that the required infrastructure needed to apply the model is very complicated. The stability analysis is typically based on velocity profiles obtained from highly resolved boundary-layer codes that must be coupled to the pressure distribution of a RANS CFD code [7]. The output of the boundary-layer method is then transferred to a stability method, which then provides information back to the turbulence model in the RANS solver. The complexity of this setup is mainly justified for special applications where the flow is designed to remain close to the stability limit for drag reduction, such as laminar wing design.

Large eddy simulation and direct numerical simulations are suitable tools for transition prediction [20], although the proper specification of the external disturbance level and structure poses substantial challenges. Unfortunately, these methods are far too costly for engineering applications. They are currently used mainly as research tools and substitutes for controlled experiments.

Despite its complexity, transition should not be viewed as outside the range of RANS methods. In many applications, transition is enforced within a narrow area of the flow due to geometric features (e.g., steps or gaps), pressure gradients, and/or flow separation. Even relatively simple models can capture these effects with sufficient engineering accuracy. The challenge to a proper engineering model is therefore mainly in the formulation of a model that can be implemented into a general RANS environment.

In this paper, a novel approach to simulating laminar to turbulent transition is described that can be implemented into a general RANS environment. The central idea behind the new approach is that Van Driest and Blumer's [21] vorticity Reynolds number concept can be used to provide a link between the transition onset Reynolds number from an empirical correlation and the local boundary-layer quantities. As a result, the model avoids the need to integrate the boundary-layer velocity profile to determine the onset of transition and this idea was first proposed by Menter et al. [22].

The vorticity or alternatively the strain-rate Reynolds number which is used in the present model is defined as follows:

$$Re_v = \frac{\rho y^2}{\mu}\left|\frac{\partial u}{\partial y}\right| = \frac{\rho y^2}{\mu} S \tag{1}$$

where y is the distance from the nearest wall. Because the vorticity Reynolds number depends only on density, viscosity, wall distance, and the vorticity (or shear strain rate), it is a local property and can be easily computed at each grid point in an unstructured, parallel Navier–Stokes code.

A scaled profile of the vorticity Reynolds number is shown in Fig. 1 for a Blasius boundary layer. The scaling is chosen to have a maximum of one inside the boundary layer. This is achieved by dividing the Blasius velocity profile by the corresponding momentum-thickness Reynolds number and a constant of 2.193. In other words, the maximum of the profile is proportional to the momentum-thickness Reynolds number and can therefore be related to the transition correlations [22] as follows:

$$Re_\theta = \frac{\max(Re_v)}{2.193} \tag{2}$$

Based on this observation, a general framework can be built, which can serve as a local environment for correlation-based transition models.

When the laminar boundary layer is subjected to strong pressure gradients, the relationship between momentum-thickness and vorticity Reynolds number described by Eq. (2) changes due to the change in the shape of the profile. The relative difference between momentum-thickness and vorticity Reynolds number, as a function of shape factor H, is shown in Fig. 2. For moderate pressure gradients ($2.3 < H < 2.9$), the difference between the actual momentum-thickness Reynolds number and the maximum of the vorticity Reynolds number is less than 10%. Based on boundary-layer analysis, a shape factor of 2.3 corresponds to a pressure gradient parameter λ_θ of approximately 0.06. Because the majority of experimental data on transition in favorable pressure gradients falls within that range (see, for example, [17]), the relative error between momentum-thickness and vorticity Reynolds number is not of great concern under those conditions.

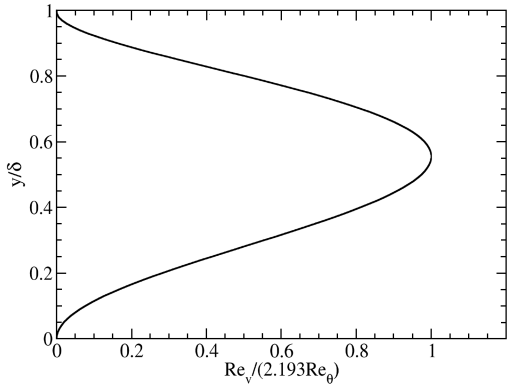

Fig. 1 Scaled vorticity Reynolds number Re_v profile in a Blasius boundary layer.

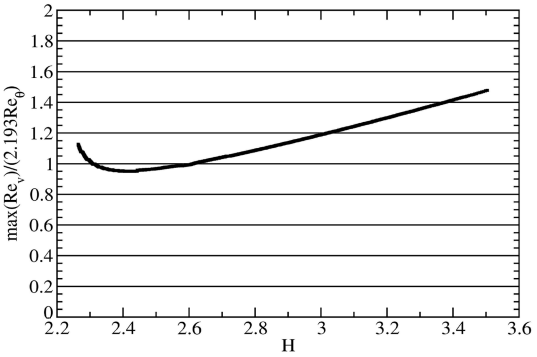

Fig. 2 Relative error between the maximum value of vorticity Reynolds number Re_v and the momentum-thickness Reynolds number Re_θ as a function of boundary-layer shape factor H.

For strong adverse pressure gradients, the difference between the momentum-thickness and vorticity Reynolds number can become significant, particularly near separation ($H = 3.5$). However, the trend with experiments is that adverse pressure gradients reduce the transition momentum-thickness Reynolds number. In practice, if a constant transition momentum-thickness Reynolds number is specified, the transition model is not very sensitive to adverse pressure gradients and an empirical correlation such as that of Abu-Ghannam and Shaw [17] is necessary to predict adverse pressure gradient transition accurately. In fact, the increase in vorticity Reynolds number with increasing shape factor can actually be used to predict separation-induced transition. This is one of the main advantages of the present approach because the standard definition of momentum-thickness Reynolds number is not suitable in separated flows.

The function Re_v can be used on physical reasoning, by arguing that the combination of $y^2 S$ is responsible for the growth of disturbances inside the boundary layer, whereas $\nu = \mu/\rho$ is responsible for their damping. As $y^2 S$ grows with the thickness of the boundary layer and μ stays constant, transition will take place once a critical value of Re_v is reached. The connection between the growth of disturbances and the function Re_v was shown by Van Driest and Blumer [21] in comparison with experimental data. As well, Langtry and Sjolander [15] found that the location in the boundary layer where Re_v was largest correspondeds surprisingly well to the location where the peak growth of disturbances was occurring, at least for bypass transition. The models proposed by Langtry and Sjolander [15] and Walters and Leylek [16], use Re_v in physics-based arguments based on these observations of disturbance growth in the boundary layer during bypass transition. These models appear superior to conventional low-Re models, as they implicitly contain information of the thickness of the boundary layer. Nevertheless, the close integration of viscous sublayer damping and transition prediction does not easily allow for an independent calibration of both submodels.

In the present approach first described in [22–25], the main idea is to use a combination of the strain-rate Reynolds number with experimental transition correlations using standard transport equations. Because of the separation of viscous sublayer damping and transition prediction, the new method has provided the flexibility for introducing additional transition effects with relative ease. Currently, the main missing extensions are crossflow instabilities and high-speed flow correlations and these do not pose any significant obstacles. The concept of linking the transition model with experimental data has proven to be an essential strength of the model and this is difficult to achieve with closures based on a physical modeling of these diverse phenomena.

The present transition model is built on a transport equation for intermittency, which can be used to trigger transition locally. In addition to the transport equation for the intermittency, a second transport equation is solved for the transition onset momentum-thickness Reynolds number. This is required to capture the non-

local influence of the turbulence intensity, which changes due to the decay of the turbulence kinetic energy in the freestream, as well as due to changes in the freestream velocity outside the boundary layer. This second transport equation is an essential part of the model as it ties the empirical correlation to the onset criteria in the intermittency equation. Therefore, it allows the model to be used in general geometries and over multiple airfoils, without additional information on the geometry. The intermittency function is coupled with the shear stress transport (SST) k-ω-based turbulence model [26]. It is used to turn on the production term of the turbulent kinetic energy downstream of the transition point based on the relation between transition momentum-thickness and strain-rate Reynolds number. As the strain-rate Reynolds number is a local property, the present formulation avoids another very severe shortcoming of the correlation-based models, namely their limitation to 2-D flows. It therefore allows the simulation of transition in 3-D flows originating from different walls. The formulation of the intermittency has also been extended to account for the rapid onset of transition caused by separation of the laminar boundary layer [Eq. (17)]. In addition, the model can be fully calibrated with internal or proprietary transition onset and transition length correlations. The correlations can also be extended to flows with rough walls or to flows with crossflow instability. It should be stressed that the proposed transport equations do not attempt to model the physics of the transition process (unlike, e.g., turbulence models), but form a framework for the implementation of correlation-based models into general-purpose CFD methods. To distinguish the present concept from physics-based transition modeling, it is called local correlation-based transition modeling.

II. Transition Model Formulation

The present transition model formulation is described very briefly for completeness; a detailed description of the model and its development can be found in Langtry [27]. It should be noted that a few changes have been made to the model since it was first published [23] to improve the predictions of natural transition. These include the following:

1) A new transition onset correlation results in improved predictions for both natural and bypass transition.

2) A modification to the separation-induced transition modification prevents it from causing early transition near the separation point.

3) Some adjustments of the model coefficients better account for flow history effects on the transition onset location.

It was expected that different groups will make numerous improvements to the model and, consequently, a naming convention was introduced in [23] to keep track of the various model versions. The basic model framework (transport equations without any correlations) was called the γ-Re_θ transition model. The version number given in [23] was called CFX-v-1.0. Based on this naming convention, the present model with the preceding modifications will be referred to as the γ-Re_θ model, CFX-v-1.1. The present transition model is briefly summarized in the following pages.

The transport equation for the intermittency γ reads

$$\frac{\partial(\rho\gamma)}{\partial t} + \frac{\partial(\rho U_j\gamma)}{\partial x_j} = P_\gamma - E_\gamma + \frac{\partial}{\partial x_j}\left[\left(\mu + \frac{\mu_t}{\sigma_f}\right)\frac{\partial\gamma}{\partial x_j}\right] \tag{3}$$

The transition sources are defined as follows:

$$P_{\gamma 1} = F_{\text{length}} c_{a1} \rho S[\gamma F_{\text{onset}}]^{0.5}(1 - c_{e1}\gamma) \tag{4}$$

where S is the strain-rate magnitude. F_{length} is an empirical correlation that controls the length of the transition region, and F_{Onset} controls the transition onset location. Both are dimensionless functions that are used to control the intermittency equation in the boundary layer. The destruction/relaminarization source is defined as follows:

$$E_\gamma = c_{a2}\rho\Omega\gamma F_{\text{turb}}(c_{e2}\gamma - 1) \tag{5}$$

where Ω is the vorticity magnitude. The transition onset is controlled by the following functions:

$$Re_V = \frac{\rho y^2 S}{\mu} \tag{6}$$

$$F_{\text{onset1}} = \frac{Re_v}{2.193 \cdot Re_{\theta c}} \tag{7}$$

$$F_{\text{onset2}} = \min(\max(F_{\text{onset1}}, F_{\text{onset1}}^4), 2.0) \tag{8}$$

$$R_T = \frac{\rho k}{\mu\omega} \tag{9}$$

$$F_{\text{onset3}} = \max\left(1 - \left(\frac{R_T}{2.5}\right)^3, 0\right) \tag{10}$$

$$F_{\text{onset}} = \max(F_{\text{onset2}} - F_{\text{onset3}}, 0) \tag{11}$$

$Re_{\theta c}$ is the critical Reynolds number where the intermittency first starts to increase in the boundary layer. This occurs upstream of the transition Reynolds number $\tilde{Re}_{\theta t}$, and the difference between the two must be obtained from an empirical correlation. Both the F_{length} and $Re_{\theta c}$ correlations are functions of $\tilde{Re}_{\theta t}$.

Based on the T3B, T3A, T3A-, and the Schubauer and Klebanof test cases [28], a correlation for F_{length} based on $Re_{\theta t}$ from an empirical correlation is defined as

$$F_{\text{length}} = \begin{cases} [398.189 \cdot 10^{-1} + (-119.270 \cdot 10^{-4})\tilde{Re}_{\theta t} + (-132.567 \cdot 10^{-6})\tilde{Re}_{\theta t}^2], & \tilde{Re}_{\theta t} < 400 \\ [263.404 + (-123.939 \cdot 10^{-2})\tilde{Re}_{\theta t} + (194.548 \cdot 10^{-5})\tilde{Re}_{\theta t}^2 + (-101.695 \cdot 10^{-8})\tilde{Re}_{\theta t}^3], & 400 \le \tilde{Re}_{\theta t} < 596 \\ [0.5 - (\tilde{Re}_{\theta t} - 596.0) \cdot 3.0 \cdot 10^{-4}], & 596 \le \tilde{Re}_{\theta t} < 1200 \\ [0.3188], & 1200 \le \tilde{Re}_{\theta t} \end{cases} \tag{12}$$

In certain cases, such as transition at higher Reynolds numbers, the $\tilde{Re}_{\theta t}$ scalar will often decrease to very small values in the boundary layer shortly after transition. Because F_{length} is based on $\tilde{Re}_{\theta t}$, this can result in a local increase in the source term for the intermittency

equation, which in turn can show up as a sharp increase in the skin friction. The skin friction does eventually return back to the fully turbulent value, however, this effect is unphysical. It appears to be caused by a sharp change in the y^+ in the viscous sublayer where the intermittency decreases back to its minimum value due to the destruction term [Eq. (5)]. The effect can be eliminated by forcing F_{length} to always be equal to its maximum value (in this case 40.0) in the viscous sublayer. The modification for doing this is shown next. The modification does not appear to have any effect on the predicted transition length. An added benefit is that, at higher Reynolds numbers, the model now appears to predict the skin friction overshoot measured by experiments:

$$F_{\text{sublayer}} = e^{-\left(\frac{R_\omega}{0.4}\right)^2} \tag{13}$$

$$R_\omega = \frac{\rho y^2 \omega}{500\mu} \tag{14}$$

$$F_{\text{length}} = F_{\text{length}}(1 - F_{\text{sublayer}}) + 40.0 \cdot F_{\text{sublayer}} \tag{15}$$

The correlation between $Re_{\theta c}$ and $\tilde{R}e_{\theta t}$ is defined as follows:

$$Re_{\theta c} = \begin{cases} [\tilde{R}e_{\theta t} - (396.035 \cdot 10^{-2} + (-120.656 \cdot 10^{-4})\tilde{R}e_{\theta t} + (868.230 \cdot 10^{-6})\tilde{R}e_{\theta t}^2 \\ \quad + (-696.506 \cdot 10^{-9})\tilde{R}e_{\theta t}^3 + (174.105 \cdot 10^{-12})\tilde{R}e_{\theta t}^4)], & \tilde{\text{Re}}_{\theta \text{t}} \le 1870 \\ [\tilde{R}e_{\theta t} - (593.11 + (\tilde{R}e_{\theta t} - 1870.0) \cdot 0.482)], & \tilde{R}e_{\theta t} > 1870 \end{cases} \tag{16}$$

The constants for the intermittency equation are

$$c_{e1} = 1.0; \qquad c_{a1} = 2.0 \qquad c_{e2} = 50; \qquad c_{a2} = 0.06; \qquad \sigma_f = 1.0$$

The modification to the intermittency for predicting separation-induced transition is

$$\gamma_{\text{sep}} = \min\left(s_1 \max\left[0, \left(\frac{Re_v}{3.235 Re_{\theta c}}\right) - 1\right] F_{\text{reattach}}, 2\right) F_{\theta t} \tag{17}$$

$$F_{\text{reattach}} = e^{-\left(\frac{R_T}{20}\right)^4} \tag{18}$$

$$\gamma_{\text{eff}} = \max(\gamma, \gamma_{\text{sep}}) \tag{19}$$

$$s_1 = 2 \tag{20}$$

The model constants in Eq. (17) have been adjusted from those of Menter et al. [23] and Langtry et al. [24] to improve the predictions of separated flow transition. See Langtry [27] for a detailed discussion of the changes to the model from the Menter et al. [23] and Langtry et al. [24] versions. The main difference is the constant that controls the relation between Re_v and $Re_{\theta c}$ was changed from 2.193, its value for a Blasius boundary layer, to 3.235, the value at a separation point where the shape factor H is 3.5 (see Fig. 2). The boundary condition for γ at a wall is zero normal flux, while for an inlet γ is equal to 1.0. An inlet γ equal to 1.0 is necessary to preserve the original turbulence model's freestream turbulence decay rate.

The transport equation for the transition momentum-thickness Reynolds number $\tilde{R}e_{\theta t}$ reads

$$\frac{\partial(\rho \tilde{R}e_{\theta t})}{\partial t} + \frac{\partial(\rho U_j \tilde{R}e_{\theta t})}{\partial x_j} = P_{\theta t} + \frac{\partial}{\partial x_j}\left[\sigma_{\theta t}(\mu + \mu_t)\frac{\partial \tilde{R}e_{\theta t}}{\partial x_j}\right] \tag{21}$$

Outside the boundary layer, the source term $P_{\theta t}$ is designed to force the transported scalar $\tilde{R}e_{\theta t}$ to match the local value of $Re_{\theta t}$ calculated from the empirical correlation [Eqs. (35) and (36)]. The source term is defined as follows:

$$P_{\theta t} = c_{\theta t}\frac{\rho}{t}(Re_{\theta t} - \tilde{R}e_{\theta t})(1.0 - F_{\theta t}) \tag{22}$$

$$t = \frac{500\mu}{\rho U^2} \tag{23}$$

where t is a time scale, which is present for dimensional reasons. The time scale was determined based on dimensional analysis with the main criteria being that it had to scale with the convective and diffusive terms in the transport equation. The blending function $F_{\theta t}$ is used to turn off the source term in the boundary layer and allow the transported scalar $\tilde{R}e_{\theta t}$ to diffuse in from the freestream. $F_{\theta t}$ is equal to zero in the freestream and one in the boundary layer. The $F_{\theta t}$ blending function is defined as follows:

$$F_{\theta t} = \min\left(\max\left(F_{\text{wake}} \cdot e^{-\left(\frac{y}{\delta}\right)^4}, 1.0 - \left(\frac{\gamma - 1/c_{e2}}{1.0 - 1/c_{e2}}\right)^2\right), 1.0\right) \tag{24}$$

$$\theta_{\text{BL}} = \frac{\tilde{R}e_{\theta t}\mu}{\rho U}; \qquad \delta_{\text{BL}} = \frac{15}{2}\theta_{\text{BL}}; \qquad \delta = \frac{50\Omega y}{U} \cdot \delta_{\text{BL}} \tag{25}$$

$$Re_\omega = \frac{\rho \omega y^2}{\mu}; \qquad F_{\text{wake}} = e^{-\left(\frac{Re_\omega}{1E+5}\right)^2} \tag{26}$$

The F_{wake} function ensures that the blending function is not active in the wake regions downstream of an airfoil/blade.

The model constants for the $\tilde{R}e_{\theta t}$ equation are

$$c_{\theta t} = 0.03; \qquad \sigma_{\theta t} = 2.0 \tag{27}$$

The boundary condition for $\tilde{R}e_{\theta t}$ at a wall is zero flux. The boundary condition for $\tilde{R}e_{\theta t}$ at an inlet should be calculated from the empirical correlation [Eqs. (35) and (36)] based on the inlet turbulence intensity.

The empirical correlation for transition onset is based on the following parameters:

$$\lambda_\theta = \frac{\rho\theta^2}{\mu}\frac{dU}{ds} \tag{28}$$

$$Tu = 100\frac{\sqrt{2k/3}}{U} \tag{29}$$

Where dU/ds is the acceleration along the streamwise direction and can be computed by taking the derivative of the velocity U in the x, y, and z directions and then summing the contribution of these derivatives along the streamwise flow direction:

$$U = (u^2 + v^2 + w^2)^{\frac{1}{2}} \tag{30}$$

$$\frac{dU}{dx} = \frac{1}{2}(u^2 + v^2 + w^2)^{-\frac{1}{2}} \cdot \left[2u\frac{du}{dx} + 2v\frac{dv}{dx} + 2w\frac{dw}{dx}\right] \quad (31)$$

$$\frac{dU}{dy} = \frac{1}{2}(u^2 + v^2 + w^2)^{-\frac{1}{2}} \cdot \left[2u\frac{du}{dy} + 2v\frac{dv}{dy} + 2w\frac{dw}{dy}\right] \quad (32)$$

$$\frac{dU}{dz} = \frac{1}{2}(u^2 + v^2 + w^2)^{-\frac{1}{2}} \cdot \left[2u\frac{du}{dz} + 2v\frac{dv}{dz} + 2w\frac{dw}{dz}\right] \quad (33)$$

$$\frac{dU}{ds} = \left[(u/U)\frac{dU}{dx} + (v/U)\frac{dU}{dy} + (w/U)\frac{dU}{dz}\right] \quad (34)$$

The use of the streamline direction is not Galilean invariant. However, this deficiency is inherent to all correlation-based models, as their main variable, the turbulence intensity, is already based on the local freestream velocity and does therefore violate Galilean invariance. This is not problematic, as the correlations are defined with respect to a wall boundary layer and all velocities are therefore relative to the wall. Nevertheless, multiple moving walls in one domain will likely require additional information.

The empirical correlation has been modified from [23] to improve the predictions of natural transition. The predicted transition Reynolds number as a function of turbulence intensity is shown in Fig. 3. For pressure gradient flows, the model predictions are similar to the Abu-Ghannam and Shaw [17] correlation. The empirical correlation is defined as follows:

$$Re_{\theta t} = \left[1173.51 - 589.428Tu + \frac{0.2196}{Tu^2}\right]F(\lambda_\theta), \quad Tu \le 1.3 \quad (35)$$

$$Re_{\theta t} = 331.50[Tu - 0.5658]^{-0.671}F(\lambda_\theta), \quad Tu > 1.3 \quad (36)$$

$$F(\lambda_\theta) = 1 - [-12.986\lambda_\theta - 123.66\lambda_\theta^2 - 405.689\lambda_\theta^3]e^{-\left[\frac{Tu}{1.5}\right]^{1.5}}, \quad \lambda_\theta \le 0 \quad (37)$$

$$F(\lambda_\theta) = 1 + 0.275[1 - e^{[-35.0\lambda_\theta]}]e^{\left[\frac{-Tu}{0.5}\right]}, \quad \lambda_\theta > 0 \quad (38)$$

For numerical robustness, the acceleration parameters, the turbulence intensity, and the empirical correlation should be limited as follows:

$$-0.1 \le \lambda_\theta \le 0.1 \qquad Tu \ge 0.027 \qquad Re_{\theta t} \ge 20$$

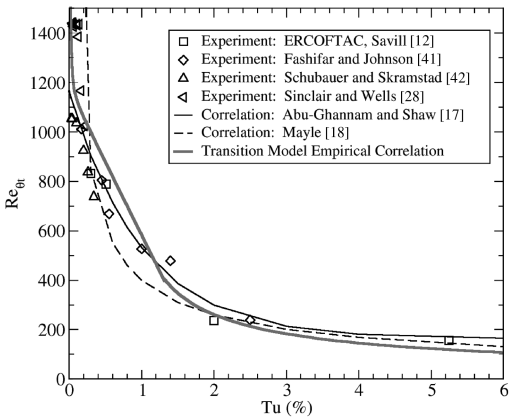

Fig. 3 Transition onset momentum-thickness Reynolds number $Re_{\theta t}$ predicted by the new correlation as a function of turbulence intensity Tu for a flat plate with zero pressure gradient.

A minimum turbulence intensity of 0.027% results in a transition momentum-thickness Reynolds number of 1450, which is the largest experimentally observed flat-plate transition Reynolds number based on the Sinclair and Wells [29] data. For cases where larger transition Reynolds number are believed to occur (e.g., aircraft in flight) this limiter may need to be adjusted downward.

The empirical correlation is used only in the source term [Eq. (22)] of the transport equation for the transition onset momentum-thickness Reynolds number. Equations. (35–38) must be solved iteratively because the momentum thickness θ_t is present in the left-hand side of the equation and also in the right-hand side in the pressure gradient parameter λ_θ. In the present work, an initial guess for the local value of θ_t was obtained based on the zero pressure gradient solution of Eqs. (35) and (36) and the local values of U, ρ, and μ. With this initial guess, Eqs. (35–38) were solved by iterating on the value of θ_t and convergence was obtained in less then 10 iterations using a shooting point method.

The transition model interacts with the SST turbulence model [26] as follows:

$$\frac{\partial}{\partial t}(\rho k) + \frac{\partial}{\partial x_j}(\rho u_j k) = \tilde{P}_k - \tilde{D}_k + \frac{\partial}{\partial x_j}\left(\left(\mu + \sigma_k \mu_t\right)\frac{\partial k}{\partial x_j}\right) \quad (39)$$

$$\tilde{P}_k = \gamma_{\text{eff}} P_k; \qquad \tilde{D}_k = \min(\max(\gamma_{\text{eff}}, 0.1), 1.0)D_k \quad (40)$$

$$R_y = \frac{\rho y\sqrt{k}}{\mu}; \qquad F_3 = e^{-\left(\frac{R_y}{120}\right)^8}; \qquad F_1 = \max(F_{1\text{orig}}, F_3) \quad (41)$$

where P_k and D_k are the original production and destruction terms for the SST model and $F_{1\text{orig}}$ is the original SST blending function. Note that the production term in the ω equation is not modified. The rationale behind the preceding model formulation is given in detail in [23].

To capture the laminar and transitional boundary layers correctly, the grid must have a y^+ of approximately one at the first grid point off the wall. If the y^+ is too large (i.e., >5), then the transition onset location moves upstream with increasing y^+. All simulations have been performed with CFX-5 using a bounded second-order upwind biased discretization for the mean flow, turbulence, and transition equations.

III. Test Cases

The remaining part of the paper will give an overview of some of the public-domain test cases that have been computed with the model described in the previous section. This naturally requires a compact representation of the simulations. Most of the cases are described in far more detail in [27], including grid refinement and sensitivity studies.

A. Flat-Plate Test Cases

The flat-plate test cases that were used to calibrate the model are the European Research Community on Flow Turbulence and Combustion (ERCOFTAC) T3 series of flat-plate experiments [12,13] and the Schubauer and Klebanoff [28] flat-plate experiment, all of which are commonly used as benchmarks for transition models. Also included is a test case in which the boundary layer experiences a strong favorable pressure gradient that causes it to relaminarize [30]. The inlet conditions for these test cases are summarized in Table 1.

The three cases T3A-, T3A, and T3B have zero pressure gradients with different freestream turbulence intensity (FSTI) levels corresponding to transition in the bypass regime. The Schubauer and Klebanof (S&K) test case [28] has a low freestream turbulence intensity and corresponds to natural transition. Figure 4 shows the comparison of the model prediction with experimental data for these cases. It also gives the corresponding FSTI values. In all simulations, the inlet turbulence levels were specified to match the experimental turbulence intensity and its decay rate. This was done by fixing the inlet turbulence intensity and, via trial and error, adjusting the inlet

Table 1 Inlet condition for the flat-plate test cases at 0.04 m upstream of plate leading edge

Case	Inlet velocity, m/s	Turbulence intensity, % Inlet/leading edge value	μ_t/μ	Density, kg/m^3	Dynamic viscosity, kg/ms
T3A	5.4	3.3	12.0	1.2	1.8×10^{-5}
T3B	9.4	6.5	100.0	1.2	1.8×10^{-5}
T3A-	19.8	0.874	8.72	1.2	1.8×10^{-5}
Schubauer and Klebanof [28]	50.1	0.3	1.0	1.2	1.8×10^{-5}
T3C2	5.29	3.0	11.0	1.2	1.8×10^{-5}
T3C3	4.0	3.0	6.0	1.2	1.8×10^{-5}
T3C4	1.37	3.0	8.0	1.2	1.8×10^{-5}
T3C5	9.0	4.0	15.0	1.2	1.8×10^{-5}
Relaminarization	1.4	5.5	15	1.2	1.8×10^{-5}

viscosity ratio (i.e., the ω inlet condition) to match the experimentally measured turbulence levels at various downstream locations. As the freestream turbulence increases, the transition location moves to lower Reynolds numbers.

The T3C test cases consist of a flat plate with a favorable and adverse pressure gradient imposed by the opposite converging/diverging wall. The wind-tunnel Reynolds number was varied for the four cases (T3C5, T3C3, T3C2, T3C4), thus moving the transition location from the favorable pressure at the beginning of the plate to the adverse pressure gradient at the end. The cases are used to demonstrate the transition models ability to predict transition under the influence of various pressure gradients. Figure 5 details the results for the pressure gradient cases. The effect of the pressure gradient on the transition length is clearly visible with favorable pressure gradients increasing the transition length and adverse pressure gradients reducing it. For the T3C4 case, the laminar boundary layer actually separates and undergoes separation-induced transition.

The relaminarization test case is shown in Fig. 6. For this case, the opposite converging wall imposes a strong favorable pressure gradient that can relaminarize a turbulent boundary layer. In both the experiment and in the CFD prediction, the boundary layer was tripped near the plate leading edge. In the CFD computation, this was accomplished by injecting a small amount of turbulent air into the boundary layer with a turbulence intensity of 3%. The same effect could have been accomplished with a small step or gap in the CFD geometry. Downstream of the trip, the boundary layer slowly relaminarizes due to the strong favorable pressure gradient.

For all of the flat-plate test cases, the agreement with the data is generally good, considering the diverse nature of the physical phenomena computed, ranging from bypass transition to natural transition, separation-induced transition, and even relaminarization.

B. Turbomachinery Test Cases

This section describes a few of the turbomachinery test cases that have been used to validate the transition model including a compressor blade, a low-pressure turbine, and a high-pressure turbine. A summary of the inlet conditions is shown in Table 2.

For the Zierke and Deutsch [31] compressor blade, transition on the suction side occurs at the leading edge due to a small leading-edge separation bubble on the suction side. On the pressure side, transition occurs at about midchord. The turbulence contours and the skin friction distribution are shown in Fig. 7. There appears to be a significant amount of scatter in the experimental data; however, overall, the transition model is predicting the major flow features correctly (i.e., fully turbulent suction side, transition at midchord on the

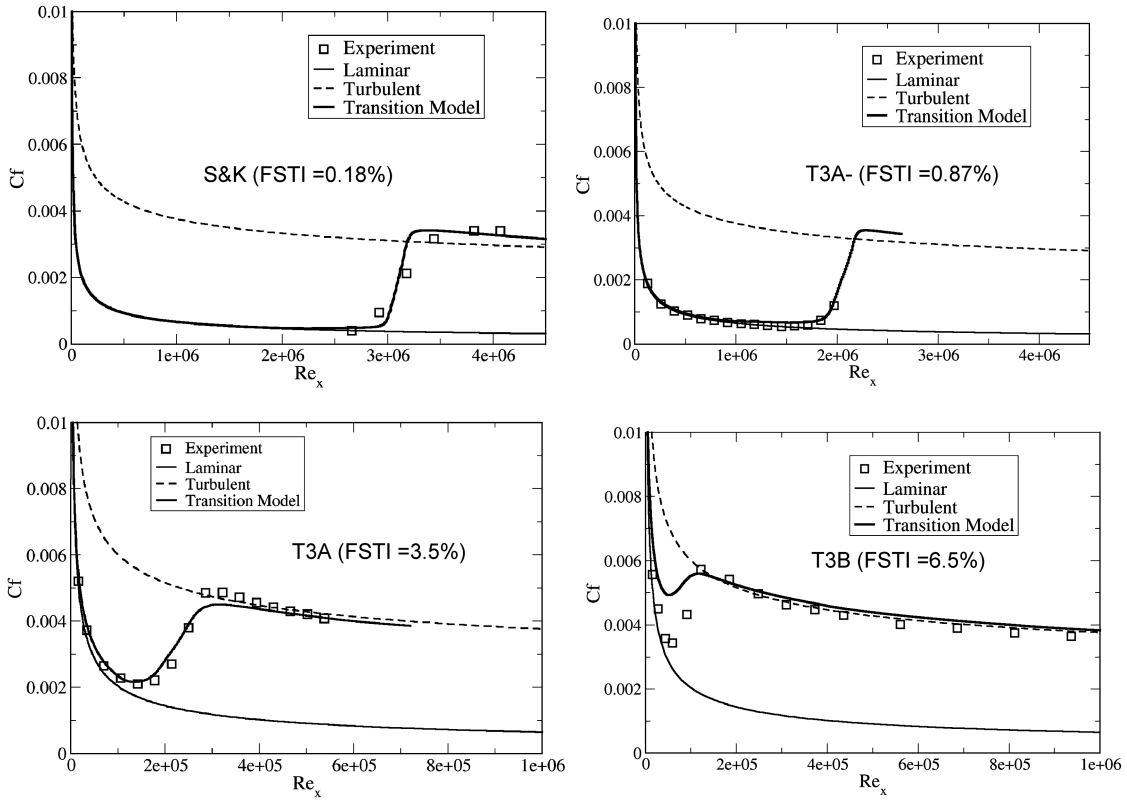

Fig. 4 Results for flat-plate test cases with different freestream turbulence levels.

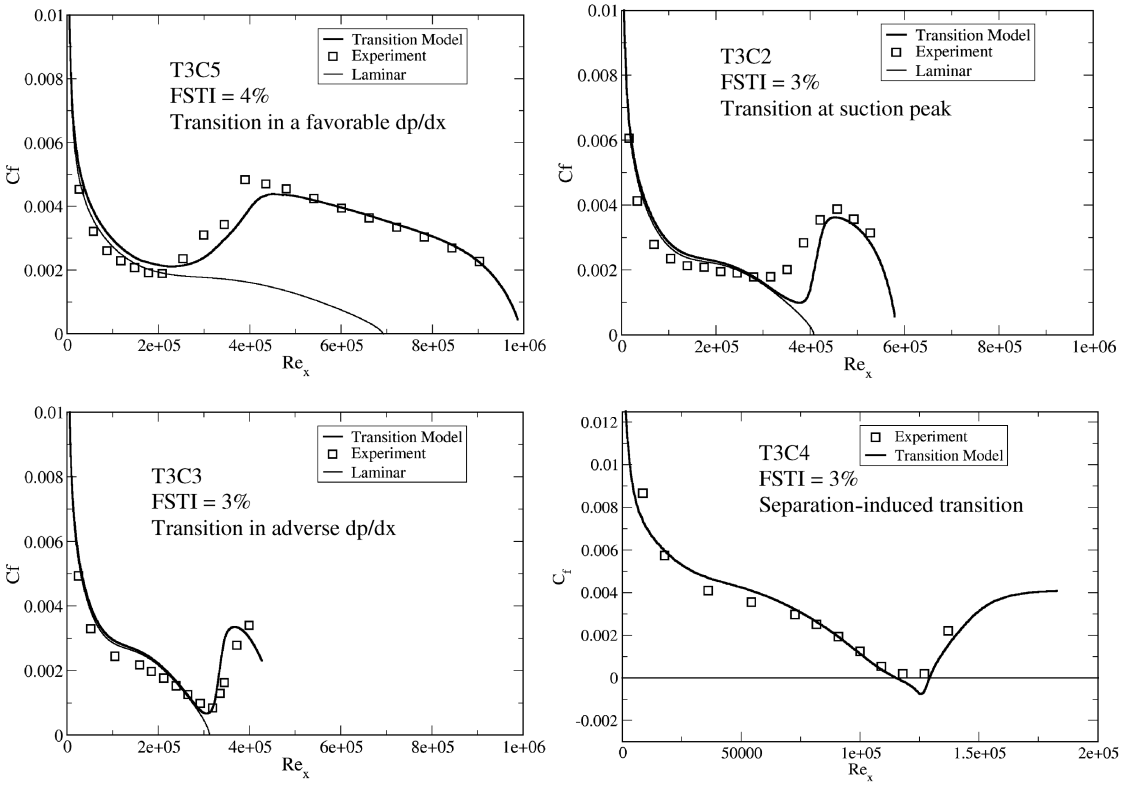

Fig. 5 Results for flat-plate test cases where variation of the tunnel Reynolds number causes transition to occur in different pressure gradients (*dp/dx*).

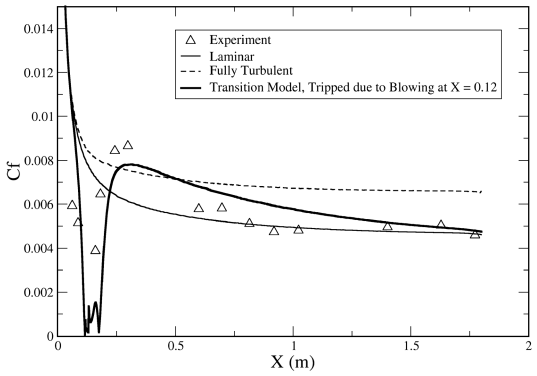

Fig. 6 Predicted skin friction C_f for a flat plate with a strong acceleration that causes the boundary layer to relaminarize.

pressure side). One important issue to note is the effect of streamwise grid resolution on resolving the leading-edge laminar separation and subsequent transition on the suction side. If the number of streamwise nodes clustered around the leading edge is too low, the model cannot resolve the rapid transition and a laminar boundary layer on the suction side is the result. For the present study, 60 streamwise nodes were used between the leading edge and the $x/C = 0.1$ location.

The Pratt and Whitney PAK-B low-pressure turbine blade is a particularly interesting airfoil because it has a loading profile similar to the rotors found in many modern aircraft engines [32]. The low-pressure rotors on modern aircraft engines are extremely challenging flowfields. This is because, in many cases, the transition occurs in the free shear layer of a separation bubble on the suction side [4]. The onset of transition in the free shear layer determines whether or not the separation bubble will reattach as a turbulent boundary layer and, ultimately, whether or not the blade will stall. The present transition model would therefore be of great interest to turbine designers if it can accurately predict the transition onset location for these types of flows.

Huang et al. [33] conducted experiments on the PAK-B blade cascade for a range of Reynolds numbers and turbulence intensities. The experiments were performed at the design incidence angle for Reynolds numbers of 50,000; 75,000; and 100,000 based on inlet velocity and axial chord length, with turbulence intensities of 0.08, 2.35, and 6.0% (which corresponded to values of 0.08, 1.6, and 2.85% at the leading edge of the blade). The computed pressure coefficient distributions obtained with the transition model and fully turbulent model are compared to the experimental data for the 75,000 Reynolds number, 2.35% turbulent intensity case in Fig. 8. On the suction side, a pressure plateau due to a laminar separation with turbulent reattachment exists. The fully turbulent computation completely misses this phenomenon because the boundary layer remains attached over the entire length of the suction surface. The transition model can predict the pressure plateau due to the laminar

Table 2 Inlet conditions for the turbomachinery test cases

Case	$Re_x = \rho c U_o/\mu$, $\times 10^6$	Mach $= U_o/a$ where speed of sound $a = (\gamma \mathrm{RT})^{0.5}$	Chord c, m	FSTI, %	μ_t/μ
Zierke and Deutsch [31] compressor incidence $= -1.5$ deg	0.47	0.1	0.2152	0.18	2.0
Pak-B low-pressure turbine blade	0.05, 0.075, 0.1	0.03	0.075	0.08, 2.35, 6.0	6.5–30
VKI MUR transonic guide vane	0.26	Inlet: 0.15 Outlet: 1.06	0.037	1.0, 6.5	11, 1000

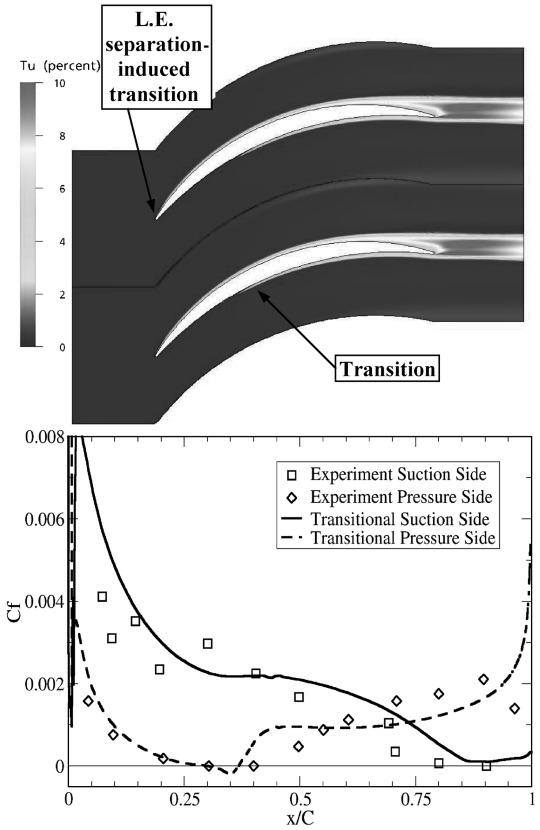

Fig. 7 Turbulence intensity contours (top) and C_f distribution against experimental data (bottom) for the Zierke and Deutsch compressor [31].

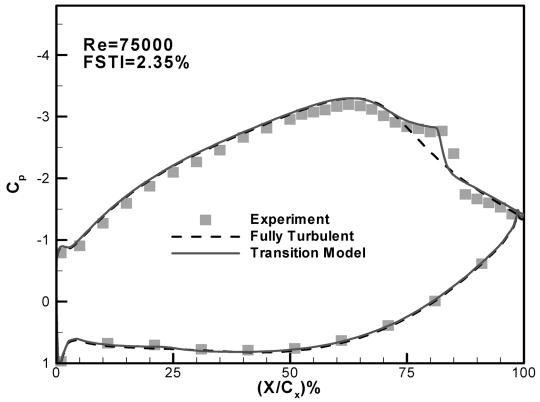

Fig. 8 Predicted blade loading for the Pak-B low-pressure turbine at a Reynolds number of 75,000 and a FSTI of 2.35%.

separation and the subsequent turbulent reattachment location. The pressure side was predicted to be fully attached and laminar.

The computed pressure coefficient distributions for various Reynolds numbers and freestream turbulence intensities compared to experimental data are shown in Fig. 9. In this figure, the comparisons are organized such that the horizontal axis denotes the Reynolds number whereas the vertical axis corresponds to the freestream turbulence intensity of the specific case. As previously pointed out, the most important feature of this test case is the extent of the separation bubble on the suction side, characterized by the plateau in the pressure distribution. The size of the separation bubble is actually a complex function of the Reynolds number and the freestream turbulence value. As the Reynolds number or freestream turbulence decrease, the size of the separation and hence the pressure plateau increases. The computations with the transition model compare well with the experimental data for all of the cases considered, illustrating the ability of the model to capture the effects of Reynolds number and turbulence intensity variations on the size of a laminar separation bubble and the subsequent turbulent reattachment.

The surface heat transfer for the transonic von Karman Institute (VKI) MUR 241 (FSTI = 6.0%) and MUR 116 (FSTI = 1.0%) test cases [34] is shown in Fig. 10. The strong acceleration on the suction side for the MUR 241 case keeps the flow laminar until a weak shock at midchord, whereas for the MUR 116 case, the flow is laminar until right before the trailing edge. Downstream of transition there appears to be a significant difference between the predicted turbulent heat transfer and the measured value. It is possible that this is the result of a Mach number (inlet Mach number $Ma_{\text{inlet}} = 0.15$, $Ma_{\text{outlet}} = 1.089$) effect on the transition length [35]. At present, no attempt has been made to account for this effect in the model. It can be incorporated in future correlations, if found consistently important.

The pressure side heat transfer is of particular interest for this case. For both cases, transition did not occur on the pressure side, however, the heat transfer was significantly increased for the high turbulence intensity case. This is a result of the large freestream levels of turbulence which diffuse into the laminar boundary layer and increase the heat transfer and skin friction. From a modeling standpoint, the effect was caused by the large freestream viscosity ratio necessary for MUR 241 to keep the turbulence intensity from decaying below 6%, which is the freestream value quoted in the experiment. The enhanced heat transfer on the pressure side was also present in the experiment and the effect appears to be physical. The model can predict this effect, as the intermittency does not multiply the eddy viscosity but only the production term of the k equation. The diffusive terms are therefore active in the laminar region.

C. Aeronautical Test Cases

This section describes a few of the aeronautical test cases that have been used to validate the transition model including a 2-D airfoil, a 2-D three-element flap, and a transonic wing. A summary of the inlet conditions is shown in Table 3.

The S809 airfoil is a 21% thick, laminar-flow airfoil that was designed specifically for horizontal-axis wind turbine applications. The airfoil profile is shown in Fig. 11. The experimental results where obtained in the low-turbulence wind tunnel at the Delft University of Technology [36,37]. The detailed CFD results can be found in [38]. The predicted pressure distribution around the airfoil for angles of attack (AoA) of 1 deg is shown in Fig. 12. For the 1 deg AoA case, the flow is laminar for the first 0.5 chord of the airfoil on both the suction and pressure sides. The boundary layers then undergo a laminar separation and reattach as a turbulent boundary layer and this is clearly visible in the experimental pressure distribution plateaus. The fully turbulent computation obviously does not capture this phenomenon, as the turbulent boundary layers remain completely attached. Both the transitional CFD and X-Foil solutions do predict the laminar separation bubble. However, X-Foil appears to slightly overpredict the reattachment location while the transitional CFD simulation is in very good agreement with the experiment.

The predicted transition locations as a function of angle of attack are shown in Fig. 13. The experimental transition locations were obtained using a stethoscope method (Somers [37]). At the moderate angles of attack, all of the results appear be to within approximately 5% chord of each other. The results obtained for the lift and drag polars are shown in Figs. 14 and 15. Between 0 and 9 deg, the lift coefficients C_l predicted by the transitional CFD and the X-Foil code are in very good agreement with the experiment, whereas the fully turbulent CFD results appear to underpredict the lift curve by approximately 0.1. Between 0 and 9 deg, the drag coefficient C_d predicted by the transitional CFD and X-Foil code are in very good agreement with the experiment, whereas the fully turbulent CFD simulation significantly overpredicts the drag, as expected.

The McDonnell Douglas 30P-30N flap configuration was originally a test case for the high-lift workshop/CFD challenge that was held at the NASA Langley Research Center in 1993 [39]. It is a very complex test case for a transition model because of the large

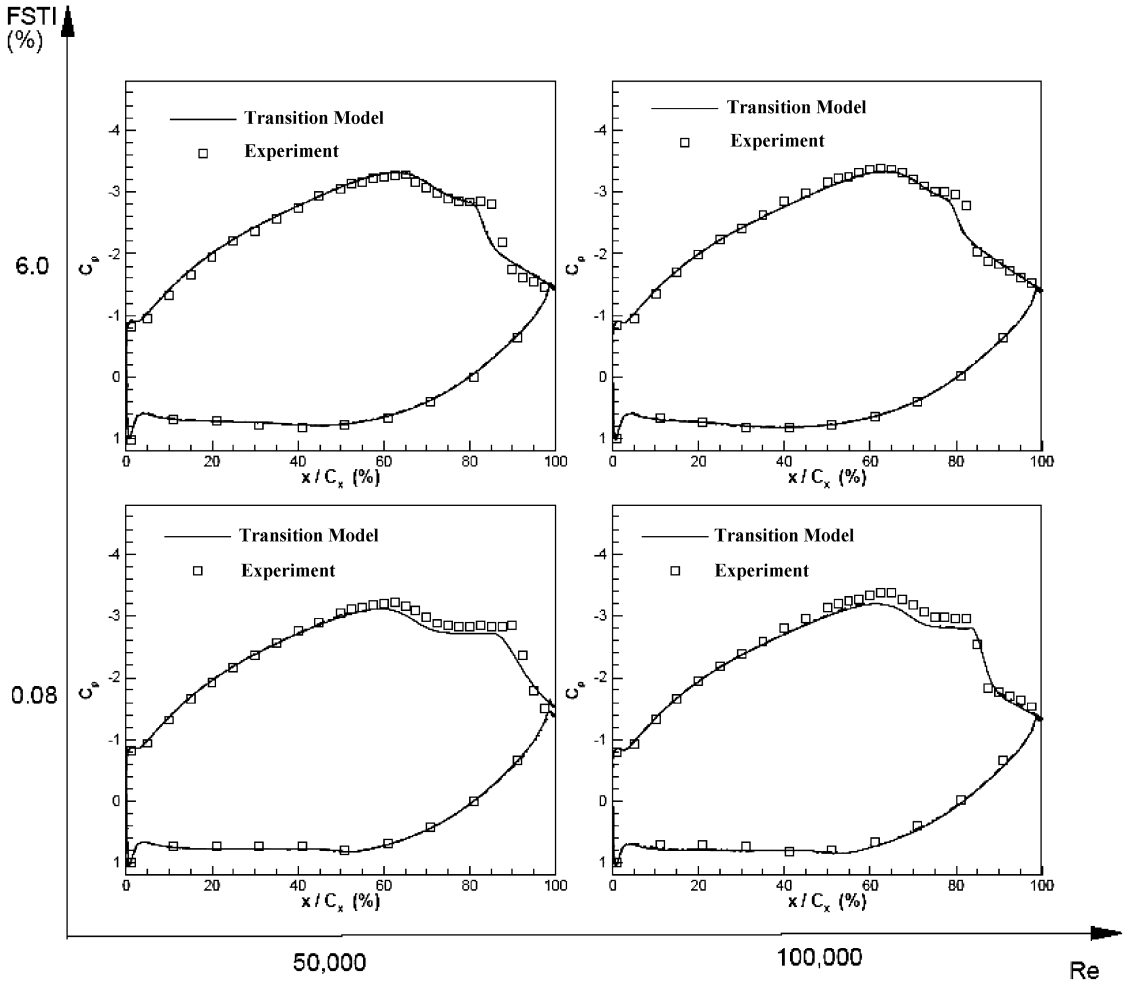

Fig. 9 Blade loading for the Pak-B low-pressure turbine at various FSTI and Reynolds numbers *Re*.

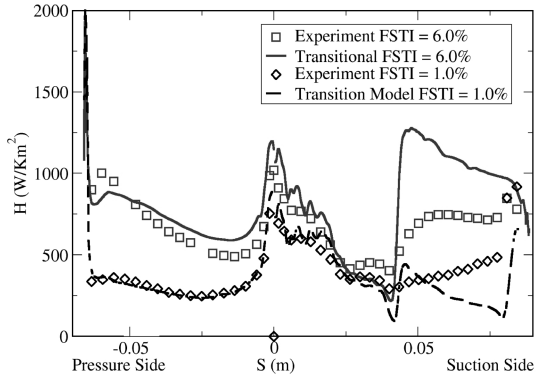

Fig. 10 Heat transfer for the VKI MUR 241 (FSTI = 6.0%) and MUR 116 (FSTI = 1.0%) test cases.

changes in pressure gradient and the varying local freestream turbulence intensity around the different lifting surfaces.

The experiment was performed in NASA Langley's low-turbulence pressure tunnel and the transition locations were measured using hot films on the upper surface of the slat and flap and on both the upper and lower surfaces of the main element. The skin friction was also measured at various locations using a Preston tube [39]. For the present comparison, the Reynolds number $Re = 9 \times 10^6$ and an angle of attack AoA = 8 deg was selected. The freestream conditions for k and ω were selected to match the transition location at the suction side of the slat. The other transition locations are an outcome of the simulation.

A contour plot of the predicted turbulence intensity around the flap is shown in Fig. 16. Also indicated are the various transition locations that were measured in the experiment (Exp.) as well as the locations predicted by the present transition model (CFD). In the computations, the onset of transition was judged as the location where the skin friction first started to increase due to the production of turbulent kinetic energy in the boundary layer. In general, the agreement between the measured and predicted transition locations is very good. The largest error was observed on the lower surface of the main element where the predicted transition location was too far downstream by approximately 6% of the cruise-airfoil chord.

The DLR F-5 geometry is a 20 deg swept wing with a symmetrical airfoil section that is supercritical at a freestream Mach number of 0.82. The experiment was performed at the DLR by Sobieczky [40] and consists of a wing mounted to the tunnel sidewall (which is

Table 3 Inlet conditions for the aeronautical test cases

Case	Re_x, $\times 10^6$	Mach	Chord, m	FSTI, %	μ_t/μ
S809 airfoil	2.0	0.1	1	0.2	10
30P-30N flap, AoA = 8.1 deg	9.0	0.2	0.5588	0.6	2.5
DLR F-5 wing, AoA = 2 deg	1.5	0.82	0.15	0.5	10

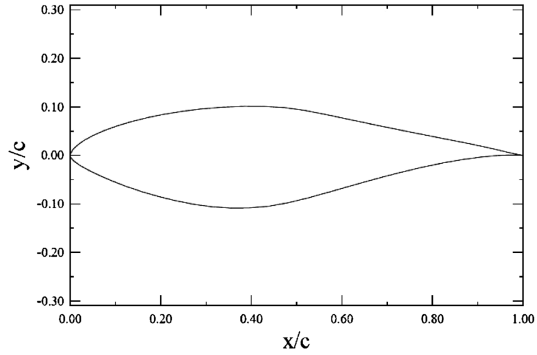

Fig. 11 S809 airfoil profile.

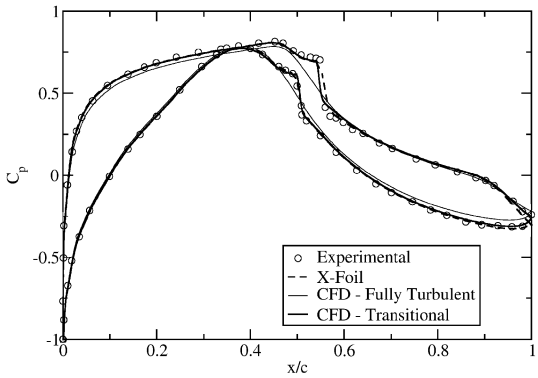

Fig. 12 Pressure distribution C_p for the S809 airfoil at 1 deg angle of attack.

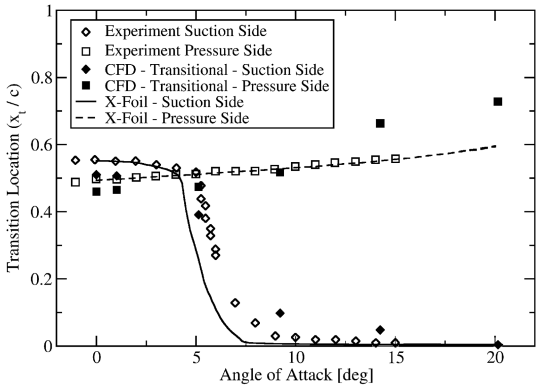

Fig. 13 Transition location (xt/c) vs angle of attack for the S809 airfoil.

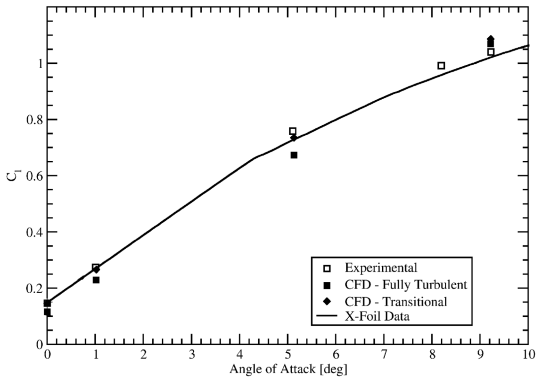

Fig. 14 Lift coefficient C_l polar for the S809 airfoil.

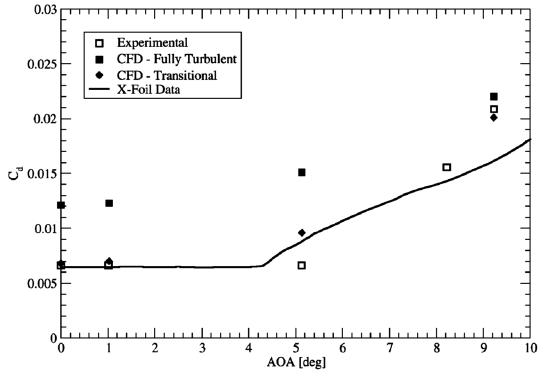

Fig. 15 Drag coefficient C_d polar for the S809 airfoil.

assumed to have transitioned far upstream of the wing). At the root, the wing was designed to blend smoothly into the wall, thus eliminating the horseshoe vortex that usually develops there. The experimental measurements consist of wing-mounted static taps at various spanwise locations and flow visualization of the surface shear using a sublimation technique. The experimental flow visualization is shown in Fig. 17 (right). Based on the flow visualization and the pressure measurements, a diagram of the flowfield around the wing was constructed and can be seen in Fig. 17 (middle). From the measurements, the boundary layer is laminar until about 60% chord where a shock causes the laminar boundary layer to separate and reattach as a turbulent boundary layer. The contours of skin friction and the surface streamlines predicted by the transition model are shown in Fig. 17 (left). From the skin friction, the laminar separation and turbulent reattachment can be clearly seen and both appear to be in good agreement with the experimental diagram from about 20% span out to the wing tip. Near the wing–body intersection, the experiments indicate earlier transition than the simulations. This might be due to the omission of the crossflow instability in the transition model.

IV. Conclusions

In this paper, various methods for transition prediction in general-purpose CFD codes have been discussed. In addition, the requirements that a model has to satisfy to be suitable for implementation into a general-purpose CFD code have been listed. The main criterion is that nonlocal operations must be avoided. A new concept of transition modeling termed local correlation-based transition model (LCTM) was introduced. It combines the advantages of locally formulated transport equations with the physical information contained in empirical correlations. The $\gamma - Re_q$ transition model is representative of that modeling concept. The model is based on two new transport equations (in addition to the k and ω equations), one for intermittency and one for a transition onset criterion in terms of momentum-thickness Reynolds number. The proposed transport equations do not attempt to model the physics of the transition process (unlike, e.g., turbulence models), but form a framework for the implementation of transition correlations into general-purpose CFD methods.

An overview of the γ-Re_q model formulation has been given along with the publication of the full model including some previously undisclosed empirical correlations that control the predicted transition length. The main goal of the present paper was to publish the full model and release it to the research community so that it can continue to be further validated and possibly extended. Included in this article are a number of test cases that can be used to validate the implementation of the model in a given CFD code.

The present transition model accounts for transition due to free-stream turbulence intensity, pressure gradients, and separation. It is fully CFD-compatible and does not negatively affect the convergence of the solver. Current limitations of the model are that crossflow instability or roughness are not included in the correlations

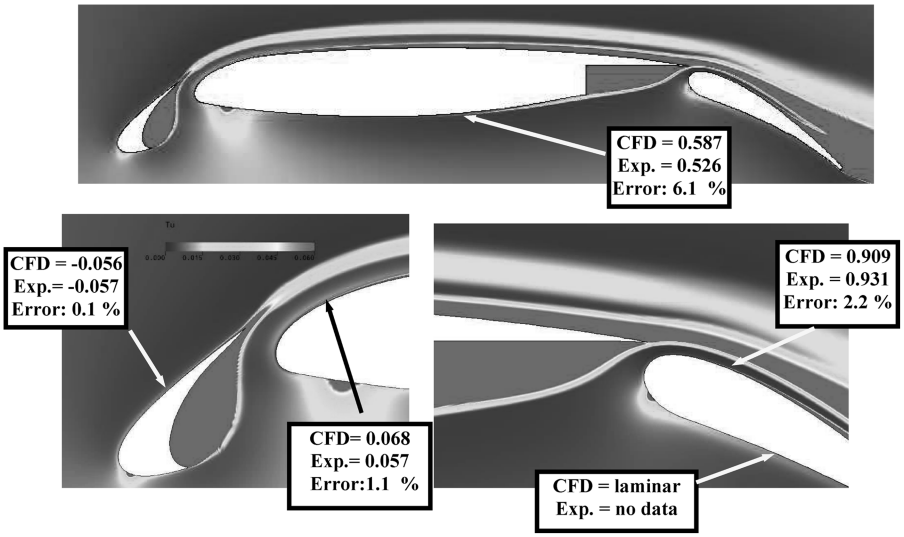

Fig. 16 Contour of turbulence intensity *Tu* around the McDonnell Douglas 30P-30N flap as well as the measured (Exp.) and predicted (CFD) transition locations (x/c) as a function of the cruise-airfoil chord ($c = 0.5588$ m). Also indicated is the relative error between the experiment and the predicted transition locations.

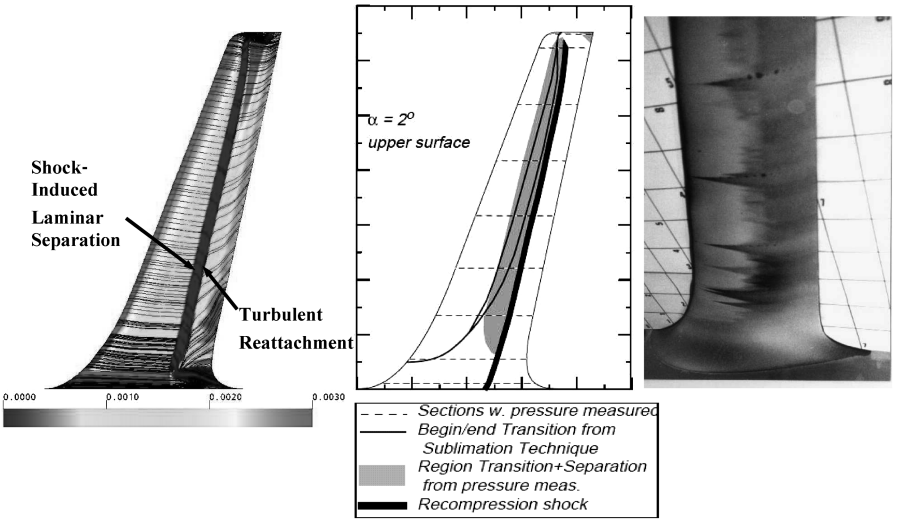

Fig. 17 DLR-F5 wing with transition: simulations (left), experiment (middle and right).

and that the transition correlations are formulated non-Galilean invariant. These limitations are currently being investigated and can be removed in principle.

An overview of the test cases computed with the new model has been given. Because of the nature of the paper, the presentation of each individual test case had to be brief. More details on the test case setup, boundary conditions, grid resolutions, etc., can be found in the literature. The purpose of the overview was to show that the model can handle a wide variety of geometries and physically diverse problems.

The authors believe that the current model is a significant step forward in engineering transition modeling. Through the use of transport equations instead of search or line-integration algorithms, the model formulation offers a flexible environment for engineering transition predictions that is fully compatible with the infrastructure of modern CFD methods. As a result, the model can be used in any general-purpose CFD method without special provisions for geometry and grid topology. The authors believe that the LCTM concept of combining transition correlations with locally formulated transport equations has a strong potential for allowing the first-order effects of transition to be included into today's industrial CFD simulations.

Acknowledgments

The model development and validation was done over the course of the first author's Ph.D. thesis and employment at ANSYS CFX. The project was funded by General Electric Aircraft Engines and General Electric Global Research, and the authors would like to thank Stefan Voelker and Bill Solomon of General Electric for their support and numerous thoughtful discussions throughout the course of the model development. We would also like to thank G. Huang of Wright State University and B. Suzen of North Dakota State University who have supported the original model development with their extensive know-how and in-house codes. Finally, the authors would also like to thank Chris Rumsey from the NASA Langley Research Center for supplying the geometry and experimental data for the McDonnell Douglas 30P-30N flap, and Helmut Sobieczky of the DLR for his helpful discussions on the DLR F-5 test case.

References

[1] Schlichting, H., *Boundary Layer Theory*, 7th ed., McGraw–Hill, New York, 1979.

[2] Morkovin, M. V., "On the Many Faces of Transition," *Viscous Drag Reduction*, edited by C. S. Wells, Plenum, New York, 1969, pp. 1–31.
[3] Malkiel, E., and Mayle, R. E., "Transition in a Separation Bubble," *Journal of Turbomachinery*, Vol. 118, No. 4, 1996, pp. 752–759.
[4] Mayle, R. E., "The Role of Laminar-Turbulent Transition in Gas Turbine Engines," *Journal of Turbomachinery*, Vol. 113, No. 4, 1991, pp. 509–537. doi:10.1115/1.2929110
[5] Smith, A. M. O., and Gamberoni, N., "Transition, Pressure Gradient and Stability Theory," Douglas Aircraft Co., Rept. ES 26388, Long Beach, CA, 1956.
[6] van Ingen, J. L., "A Suggested Semi-Empirical Method for the Calculation of the Boundary Layer Transition Region," Univ. of Delft, Dept. Aerospace Engineering, Rept. VTH-74, Delft, The Netherlands, 1956.
[7] Stock, H. W., and Haase, W., "Navier-Stokes Airfoil Computations with e^N Transition Prediction Including Transitional Flow Regions," *AIAA Journal*, Vol. 38, No. 11, 2000, pp. 2059–2066. doi:10.2514/2.893
[8] Drela, M., and Giles, M. B., "Viscous-Inviscid Analysis of Transonic and Low Reynolds Number Airfoils," *AIAA Journal*, Vol. 25, No. 10, 1987, pp. 1347–1355. doi:10.2514/3.9789
[9] Youngren, H., and Drela, M., "Viscous-Inviscid Method for Preliminary Design of Transonic Cascades," AIAA Paper No. 91-2364, 1991.
[10] Jones, W. P., and Launder, B. E., "The Calculation of Low Reynolds Number Phenomena with a Two-Equation Model of Turbulence," *International Journal of Heat and Mass Transfer*, Vol. 16, 1973, pp. 1119–1130. doi:10.1016/0017-9310(73)90125-7
[11] Rodi, W., and Scheuerer, G., "Calculation of Laminar-Turbulent Boundary Layer Transition on Turbine Blades," AGARD CP 390, 1984.
[12] Savill, A. M., "Some Recent Progress in the Turbulence Modeling of By-Pass Transition," *Near-Wall Turbulent Flows*, edited by R. M. C. So, C. G. Speziale, and B. E. Launder, Elsevier, New York, 1993, p. 829.
[13] Savill, A. M., *One-Point Closures Applied to Transition, Turbulence and Transition Modeling*, edited by M. Hallbäck, Kluwer, Dordrecht, The Netherlands, 1996, pp. 233–268.
[14] Wilcox, D. C. W., "Simulation of Transition with a Two-Equation Turbulence Model," *AIAA Journal*, Vol. 32, No. 2, 1994, pp. 247–255. doi:10.2514/3.59994
[15] Langtry, R. B., and Sjolander, S. A., "Prediction of Transition for Attached and Separated Shear Layers in Turbo Machinery," AIAA Paper 2002-3643, 2002.
[16] Walters, D. K., and Leylek, J. H., "A New Model for Boundary-Layer Transition Using a Single-Point RANS Approach," American Society of Mechanical Engineers, IMECE2002-HT-32740, 2002.
[17] Abu-Ghannam, B. J., and Shaw, R., "Natural Transition of Boundary Layers: The Effects of Turbulence, Pressure Gradient, and Flow History," *Journal of Mechanical Engineering Science*, Vol. 22, No. 5, 1980, pp. 213–228. doi:10.1243/JMES_JOUR_1980_022_043_02
[18] Mayle, R. E., "The Role of Laminar-Turbulent Transition in Gas Turbine Engines," *Journal of Turbomachinery*, Vol. 113, No. 4, 1991, pp. 509–537. doi:10.1115/1.2929110
[19] Suzen, Y. B., Huang, P. G., Hultgren, L. S., and Ashpis, D. E., "Predictions of Separated and Transitional Boundary Layers Under Low-Pressure Turbine Airfoil Conditions Using an Intermittency Transport Equation," *Journal of Turbomachinery*, Vol. 125, No. 3, July 2003, pp. 455–464. doi:10.1115/1.1580159
[20] Durbin, P. A., Jacobs, R. G., and Wu, X., "DNS of Bypass Transition," *Closure Strategies for Turbulent and Transitional Flows*, edited by B. E. Launder, and N. D. Sandham, Cambridge Univ. Press, Cambridge, England, U.K., 2002, pp. 449–463.
[21] Van Driest, E. R., and Blumer, C. B., "Boundary Layer Transition: Freestream Turbulence and Pressure Gradient Effects," *AIAA Journal*, Vol. 1, No. 6, June 1963, pp. 1303–1306. doi:10.2514/3.1784
[22] Menter, F. R., Esch, T., and Kubacki, S., "Transition Modelling Based on Local Variables," *Proceedings of the 5th International Symposium on Engineering Turbulence Modelling and Measurements*, Elsevier, Amsterdam, 2002, pp. 555–564.
[23] Menter, F. R., Langtry, R. B., Likki, S. R., Suzen, Y. B., Huang, P. G., and Völker, S., "A Correlation Based Transition Model Using Local Variables Part 1: Model Formulation," *Journal of Turbomachinery*, Vol. 128, No. 3, 2006, pp. 413–422.
[24] Langtry, R. B., Menter, F. R., Likki, S. R., Suzen, Y. B., Huang, P. G., and Völker, S., "A Correlation Based Transition Model Using Local Variables Part 2: Test Cases and Industrial Applications," *Journal of Turbomachinery*, Vol. 128, No. 3, 2006, pp. 423–434. doi:10.1115/1.2184353
[25] Menter, F. R., Langtry, R. B., and Völker, S., "Transition Modelling for General Purpose CFD Codes," *Flow, Turbulence and Combustion*, Vol. 77, Nos. 1–4, 2006, pp. 277–303. doi:10.1007/s10494-006-9047-1
[26] Menter, F. R., "Two-Equation Eddy-Viscosity Turbulence Models for Engineering Applications," *AIAA Journal*, Vol. 32, No. 8, 1994, pp. 1598–1605. doi:10.2514/3.12149
[27] Langtry, R. B., "A Correlation-Based Transition Model Using Local Variables for Unstructured Parallelized CFD Codes," Ph.D. Thesis, Univ. of Stuttgart, Stuttgart, Germany, 2006, http://elib.uni-stuttgart.de/opus/volltexte/2006/2801/.
[28] Schubauer, G. B., and Klebanoff, P. S., "Contribution on the Mechanics of Boundary Layer Transition," NACA TN 3489, 1955.
[29] Sinclair, C., and Wells, C. S., Jr., "Effects of Freestream Turbulence on Boundary-Layer Transition," *AIAA Journal*, Vol. 5, No. 1, 1967, pp. 172–174. doi:10.2514/3.3931
[30] McIlroy, H. M., and Budwig, R. S., "The Boundary Layer over Turbine Blade Models with Realistic Rough Surfaces," *ASME Turbo Expo*, American Society of Mechanical Engineers, GT2005-68342, 2005.
[31] Zierke, W. C., and Deutsch, S., "The Measurement of Boundary Layers on a Compressor Blade in Cascade," Vols. 1–2, NASA CR 185118, 1989.
[32] Dorney, D. J., Lake, J. P., King, P. L., and Ashpis, D. E., "Experimental and Numerical Investigation of Losses in Low-Pressure Turbine Blade Rows," AIAA Paper AIAA-2000-0737, 2000.
[33] Huang, J., Corke, T. C., Thomas, F. O., "Plasma Actuators for Separation Control of Low Pressure Turbine Blades," AIAA Paper No. AIAA-2003-1027, 2003.
[34] Arts, T., Lambert de Rouvroit, M., and Rutherford, A. W., "Aero-Thermal Investigation of a Highly Loaded Transonic Linear Turbine Guide Vane Cascade," von Karman Inst. for Fluid Dynamics, TN 174, 1990.
[35] Steelant, J., and Dick, E., "Modeling of Laminar-Turbulent Transition for High Freestream Turbulence," *Journal of Fluids Engineering*, Vol. 123, No. 1, 2001, pp. 22–30. doi:10.1115/1.1340623
[36] Somers, D. M., "Design and Experimental Results for the S809 Airfoil," Airfoils, Inc., State College, PA, 1989.
[37] Somers, D. M., "Design and Experimental Results for the S809 Airfoil," National Renewable Energy Lab., SR-440-6918, Jan. 1997.
[38] Langtry, R. B., Gola, J., and Menter, F. R., "Predicting 2-D Airfoil and 3-D Wind Turbine Rotor Performance Using a Transition Model for General CFD Codes," AIAA Paper 2006-0395, 2006.
[39] Klausmeyer, S. M., and Lin, J. C., "Comparative Results from a CFD Challenge over a 2-D Three-Element High-Lift Airfoil," NASA, TM 112858, 1997.
[40] Sobieczky, H., "DLR, F5: Test Wing for CFD and Applied Aerodynamics," Test Case B-5 in *AGARD FDP Advisory Rept. AR 303: Test Cases for CFD Validation*, AGARD, 1994.
[41] Fashifar, A., and Johnson, M. W., "An Improved Boundary Layer Transition Correlation," American Society of Mechanical Engineers Paper ASME-92-GT-245, 1992.
[42] Schubauer, G. B., and Skramstad, H. K., "Laminar-Boundary-Layer Oscillations and Transition on a Flat Plate," NACA Rept. 909, 1948.

M. Glauser
Associate Editor